Impact of thrombus composition on virtual thrombectomy procedures using human clot analogues mechanical data

Fregona, Virginia; Luraghi, Giulia; Fereidoonnezhad, Behrooz; Gijsen, Frank J.H.; Majoie, Charles B.L.M.; Rodríguez Matas, Jose Felix; Migliavacca, Francesco

DOI
10.1016/j.jmbbm.2025.106886

Publication date
2025

Document Version
Final published version

Published in
Journal of the mechanical behavior of biomedical materials

journal of the mechanical behavior of biomedical materials 163 (2025) 106886

Contents lists available at ScienceDirect

Journal of the Mechanical Behavior of Biomedical Materials

journal homepage: www.elsevier.com/locate/jmbbm

Impact of thrombus composition on virtual thrombectomy procedures using human clot analogues mechanical data

Virginia Fregona [a], Giulia Luraghi [a,b,*], Behrooz Fereidoonnezhad [b], Frank J.H. Gijsen [b,c], Charles B.L.M. Majoie [d], Jose Felix Rodríguez Matas [a], Francesco Migliavacca [a]

[a] Department of Chemistry, Materials and Chemical Engineering 'Giulio Natta', Politecnico di Milano, Italy
[b] Department of Biomechanical Engineering, Delft University of Technology, Delft, the Netherlands
[c] Department of Biomedical Engineering, Erasmus MC, Rotterdam, the Netherlands
[d] Department of Radiology and Nuclear Medicine, Amsterdam UMC, Location University of Amsterdam, Amsterdam, the Netherlands

ARTICLE INFO

Keywords:
Thrombectomy
Acute ischemic stroke
In silico medicine
Digital twin in healthcare
Finite element analysis

ABSTRACT

Endovascular thrombectomy (EVT) aims at restoring blood flow in case of acute ischemic stroke by removing the thrombus occluding a large cerebral artery. During the procedure with stent-retriever, the thrombus is captured within the device, which is then retrieved, subjecting the thrombus to several forces, potentially leading to its fragmentation. *In silico* studies, along with mechanical characterisation of thrombi, can enhance our understanding of the EVT, helping the development of new devices and interventional strategies. Our group previously validated a numerical approach to study EVT able to account for thrombus fragmentation. In this study, the same methodology was employed to explore the applicability of the chosen failure criterion to EVT simulations and the impact of thrombus composition on the outcome of the *in silico* procedure. For the first time, human clot analogues experimental data were applied to this methodology. Clot analogues of three different compositions were tested, and a material model incorporating failure was calibrated, followed by a verification analysis. Finally, the calibrated material model was used to perform EVT simulations, combining the three tested thrombus compositions with three different stent retriever models. The experimental tests confirmed a compression-tension asymmetry in the stress-strain curves, showing decreasing stiffness with increasing the red blood cell (RBC) content. Applying the resulting material models to EVT simulations demonstrated: (i) the dependency of the failure criterion on the thrombus mesh size, (ii) a greater tendency for RBC-rich thrombi to fragment, and (iii) increased difficulty in retrieving RBC-poor thrombi compared to RBC-rich thrombi.

1. Introduction

Acute ischemic stroke (AIS), constituting the 65.3% of strokes (Feigin et al., 2024a), is a condition where a thrombus occludes a cerebral vessel, resulting in a reduced blood flow to the downstream areas of the brain (Chugh, 2019). If blood flow is not restored as soon as possible, brain tissue can be permanently damaged, with severe consequences on the patient's life expectancy. Indeed, it is the third-leading cause of disability and mortality in the world (Abbafati et al., 2020), causing in 2021 the 10.7% of all deaths and the 5.6% of disability-adjusted life-year (Feigin et al., 2024b). Over the last two decades the endovascular thrombectomy (EVT) has been introduced and it has become the standard of care in case of large vessel occlusion (Berkhemer et al., 2015; Chalumeau et al., 2018; Goyal et al., 2015; Jovin et al., 2015; Saver et al., 2015), being the rate of substantial reperfusion around 70%–80% (Yoo and Andersson, 2017). EVT involves the mechanical removal of the thrombus using stent-retrievers and/or aspiration catheters. In case of EVT with stent-retrievers only, the stent-retriever —a self-expandable stent made of a Nickel-Titanium alloy connected to a wire for the retrieval — is navigated up to the occlusion site while crimped in a microcatheter. After being placed across the occlusion, the stent-retriever is deployed by withdrawing the microcatheter. During deployment the thrombus is engaged by the structure of the stent-retriever. The stent-retriever, along with the captured thrombus, is then retrieved by pulling the wire.

Thrombi are formed by red blood cells (RBCs), entrapped in a fibrous

* Corresponding author. Computational Biomechanics Laboratory – LaBS Department of Chemistry, Materials and Chemical engineering "Giulio Natta" Politecnico di Milano, Piazza L. da Vinci 32, 20133, Milano, Italy.
E-mail address: giulia.luraghi@polimi.it (G. Luraghi).

https://doi.org/10.1016/j.jmbbm.2025.106886
Received 24 September 2024; Received in revised form 14 December 2024; Accepted 1 January 2025
Available online 2 January 2025

network of fibrin and platelets (Staessens and De Meyer, 2021). Histological analysis of thrombi retrieved from acute ischemic stroke patients showed that the RBCs content spanned from 0% to 90% (Boodt et al., 2021; Boeckh-Behrens et al., 2016; Kim et al., 2015; Ye et al., 2021; Sporns et al., 2019). This variability is clinically significant, as clinical data show that fibrin-rich thrombi are more difficult to retrieve (Yuki et al., 2012), while RBCs-rich thrombi are more prone to fragmentation (Kaesmacher et al., 2017). This suggests that the different thrombus composition influences the interaction between thrombus and stent-retriever, as well as the procedural outcome. Moreover, studies assessing the mechanical behaviour of either retrieved AIS thrombi or clot analogues (made from animal or human blood), showed that the composition of a thrombus has an impact on its mechanical behaviour (Cahalane et al., 2021). The most common test is the unconfined compression, which was performed on ovine clot analogues (Johnson et al., 2020, 2021; Fereidoonnezhad et al., 2021), porcine clot analogues (Chueh et al., 2011; Krasokha et al., 2010), bovine clot analogues (Chueh et al., 2011; Malone et al., 2018), and human clot analogues (Liang et al., 2017; Krasokha et al., 2010; Cruts et al., 2023; Cahalane et al., 2023, 2024). This type of test is feasible also on retrieved human thrombi, which can be trimmed to achieve a suitable shape for testing (Boodt et al., 2021). A general result of compression test is the observation of a non-linear stress-strain behaviour. Tensile tests are less frequent due to the difficulty in handling and gripping samples, and the necessity of samples of a more complex shape (e.g. dogbone). Examples are the works by Krasokha et al. (2010) on porcine clot analogues, Malone et al. (2018) on bovine clot analogues, and by Y. Liu et al. (2020); Cahalane et al. (2023) on human clot analogues. However, including the tensile test in the mechanical characterisation is important due to the observed asymmetric behaviour of thrombi in compression and tension (Cahalane et al., 2023). Regarding the correlation between thrombus composition and its mechanical properties, literature suggests that an increase in RBCs content is linked to a decrease in thrombus stiffness (Boodt et al., 2021) (Y. Liu et al., 2020; Cahalane et al., 2023).

A crucial aspect in the interpretation of the results of mechanical testing on clot analogues is the concept of 'contraction' of the clot, which is the last stage of clot maturation (Litvinov and Weisel, 2023). In this phenomenon the activated platelets bend individual fibrin fibres, causing the increase of fibrin network density and, as a consequence, the volume shrinkage and the stiffening of the clot (Kim et al., 2017); contemporarily, there is the expulsion of serum from the clot (Cines et al., 2014). Since the presence of RBCs hinders the full contraction of the clot, the amount of clot contraction is inversely proportional to the haematocrit (Tutwiler et al., 2016; Johnson et al., 2020). As a consequence of this process, as observed in Cahalane et al. (2023); Cruts et al. (2023), the percent volume of RBCs in the blood mixture is lower than the one in the final clot analogue (Kim et al., 2017; Johnson et al., 2020; Litvinov and Weisel, 2023). For instance, in Cahalane et al. (2023) the 40% RBCs in the blood mixture led to about 90% RBCs in the contracted clot, while the 5% RBCs already led approximately to a 70% RBCs clot, which can be already classified as a RBCs-rich clot.

In silico studies have a great potential to enhance our understanding of the thrombus removal during the EVT procedure. Since the clinical procedure is relatively new, there are not many examples of *in silico* EVT with stent-retriever in the literature. The first finite element analysis (FEA) by Gu et al. (2017) was focused on the stent-retriever in a simplified vessel geometry, modelling the thrombus as a bullet-shaped, hyperelastic incompressible material. Another example by Liu et al. (2022) simplified the vessels into a plane, and the thrombus was modelled as a cylinder with a dome on both sides. A hyperelastic material model calibrated on compression test data was assigned to the thrombus. Mousavi et al. (2021) simulated a EVT procedure in a rigid cylindrical vessel. A first-order Ogden hyperelastic constitutive model was assigned to the thrombus and a combination of finite elements (FE) and smoothed particle hydrodynamics was used to account for the large deformations of the thrombus as well as the penetration of the stent-retriever in the thrombus. Aiming to replicate the procedure in more realistic conditions, our group developed and validated the first FEA in which the whole procedure (stent-retriever crimping, tracking, deployment, and retrieval) was replicated in realistic vessel morphologies, firstly using *in vitro* tests (Luraghi et al., 2021a), and then clinical data of a patient-specific case (Luraghi et al., 2021b). In these studies, calibration of the adopted quasi-hyperelastic material model were carried out with compression and tension test data of ovine clot analogues and of *ex-vivo* thrombi. To obtain a more realistic modelling of the thrombus behaviour, a first attempt of including a thrombus failure criterion was made (Luraghi et al., 2022a). However, while thrombus fracture is studied in the literature (Fereidoonnezhad et al., 2021a,b; Tutwiler et al., 2020, 2021; Liu et al., 2021, 2024; Sugerman et al., 2020; Lohr et al., 2024; Gültekin et al., 2024), the inclusion of fracture in the *in silico* EVT is still an open challenge, due to the limited number of failure models compatible with the FEA of the whole EVT procedure, where mixed fracture modes are involved and the fracture propagation does not follow a predictable path.

The aim of this work is to introduce in our validated methodology replicating the EVT procedure a material model with failure calibrated, for the first time, on human clot analogues data. This is done to study: (i) how the chosen failure criterion is applicable to the EVT simulation, and (ii) how thrombus composition impacts the outcome of the *in silico* procedure. *In silico* simulations, indeed, enable changing thrombus composition while keeping the same vessel geometry, device, and EVT procedure, to compare the outcomes in terms of success or unsuccess, and, with the introduction of the fragmentation, also in terms of amount of generated fragments. Firstly, knowing the importance of having both compression and tensile data due to the stress-strain curve asymmetry, a mechanical characterisation of human clot analogues in compression and tension until rupture is performed. Secondly, a material model including failure is calibrated to replicate *in silico* the experimental tests. Thirdly, a verification analysis is conducted on the failure criterion to assess its applicability in the EVT simulation. Finally, EVT simulations are run in a patient-like cerebral anatomy with the combination of three thrombus compositions and three stent-retriever models.

2. Methods

2.1. Clot modelling

2.1.1. Experimental characterisation of clot analogues

Six human clot analogues were prepared from the blood of one healthy donor with the protocol described in Cahalane et al. (2023) and reported for completeness in Appendix A. Briefly, the process of clot analogues creation started within 1 h from the blood draw. After the separation of plasma and RBCs, they were mixed to obtain three different volumetric percentages of RBCs: 0%, 1%, and 40%, to test fibrin-rich, intermediate composition, and RBCs-rich clot analogues (Cahalane et al., 2023). Clot analogues were created by adding thrombin to the blood mixture, which was then placed into syringes for compression samples and into dogbone-shaped moulds for tensile samples. After the clot maturation overnight, tensile samples were removed from their mould, while compression samples were obtained cutting the cylindrical clot created in the syringes at 2 mm of height. The compression test was conducted up to 80% strain, whereas the tensile test was conducted up to failure. Both tests were conducted at 10% strain/s. Due to the different geometries of the samples (Fig. 1a–b), two different strategies were exploited for measuring their cross-sections and reconstructing models for simulation: perpendicular pictures were taken from above the compression samples (Fig. 1a), and ultrasound imaging was used for the tensile samples. The ultrasound imaging involved capturing 20 cross-sections along each sample (Fig. 1c), which were subsequently averaged.

The Poisson's ratio was estimated from the pictures of the sample taken during the tensile test as explained in Appendix A. The initial and

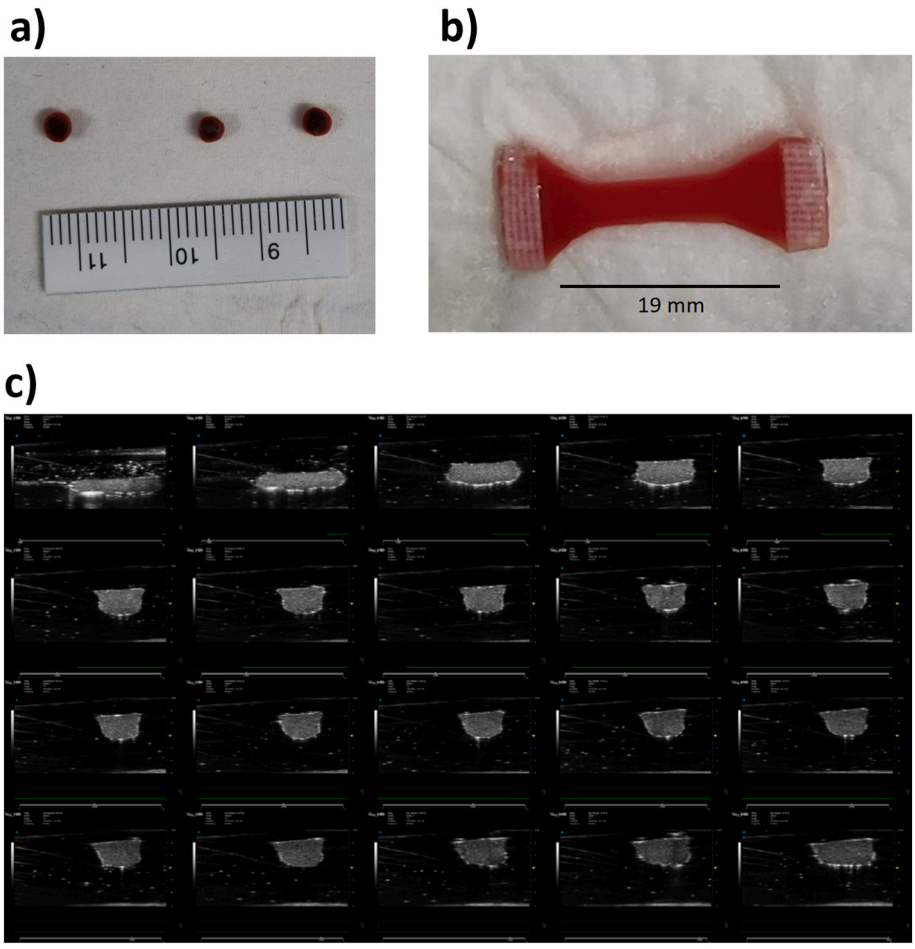

Fig. 1. a) Three 1% RBCs compression samples photographed from above next to a ruler. b) 1% RBCs dog-bone shaped tensile sample. c) Ultrasound images of the 1% RBCs sample.

final lengths of the sample, as well as the initial and final widths halfway along its length were measured and the Poisson's ratio was calculated as the inverse of the ratio between the transverse strain and the longitudinal strain. For each sample and direction three measurements were taken and averaged. All measurements were performed with the software ImageJ (National Institutes of Health, USA).

2.1.2. *In silico replica of the experimental tests*

To accurately replicate the experimental tests *in silico*, the geometry of the samples had to be reconstructed as closely as possible, to correctly compute the stresses. For the compression samples, the cross-section was reconstructed with the software ImageJ and then extruded to the sample's height (2 mm in all cases). For the tensile samples, segmentation of ultrasound images was performed using ImageJ and 3D Slicer software (Brigham and Women's Hospital, Harvard University and NIH, USA).

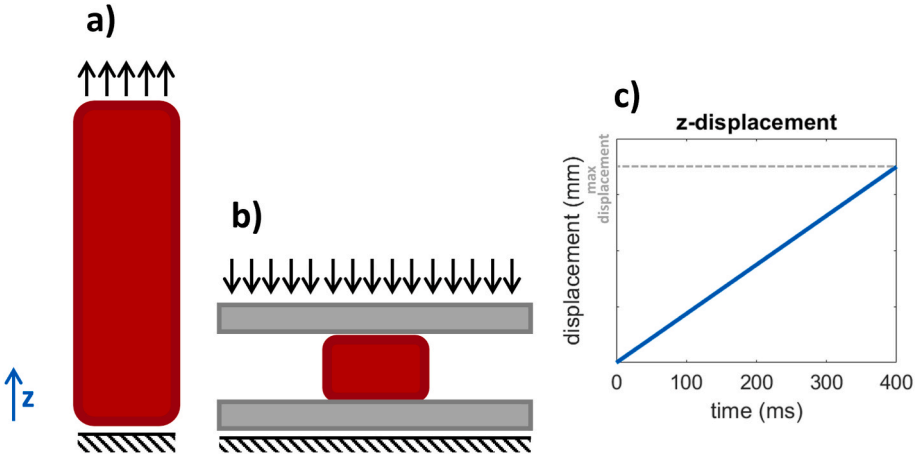

Fig. 2. Boundary conditions for the *in silico* replica of the experimental tests for a) the tensile test b) the compression test. c) Curve of the z-displacement against time given as a boundary condition to the upper face of the clot for the tensile test and to the upper plate for the compression test.

The models were meshed using ANSA (BetaCAE System, Switzerland) software with 0.2 mm tetrahedral elements for the compression samples and 0.3 mm tetrahedral elements for the tensile samples, whose dimensions were chosen after a mesh sensitivity analysis (Appendix C).

The experimental compression and tensile tests were replicated *in silico* using the explicit finite element solver LS-DYNA (Ansys, Canonsburg, PA, USA). For the compression tests, displacement boundary conditions were applied on two plates, while for the tensile tests they were applied directly to the two ends of the sample. In both cases the displacement of one side (lower face or lower plate for tensile and compression test, respectively) were blocked, while a ramp of displacement was applied to the other side (upper face or upper plate) to replicate the experimental tests (Fig. 2). For compression the maximum displacement was set to −1.6 mm, in order to reach a maximum nominal strain of 80%, as in the experimental test. For tension, the maximum displacement was set in order to obtain a maximum strain of 200% for the 0% and 1% RBCs, and a maximum strain of 100% for the 40% RBCs, to reach a maximum strain higher than the failure strain of the experimental tests.

Regarding the clot, one of the disadvantages of classical hyperelastic models is the identification of the material parameters that is usually quite complex. In addition, in many biological tissues like the material of the clot featuring different initial moduli in tension and compression (or a fast transition between tension and compression), classical hyperplastic models with parameters obtained by a least squares fit can never produce an exact fit, whereas this poses no problem for the tabulated model used in this work (Kolling et al., 2007). In this regard, the clot was assigned a tabulated model implemented in LS-DYNA (based on the work by Kolling et al.) which does not require continuity in the derivative of the stress-strain curve but only continuity of the stress as a function of the strain. In addition, only uniaxial stress-strain data is needed to setup the material model (see Appendix B).

To replicate the fracture of the experimental samples, a failure criterion, based on the definition of a threshold value of the maximum principal stress (PSMAX) (Luraghi et al., 2022a,b), was employed. When an element exceeds this threshold, it is cancelled from the calculation, creating discontinuities and eventually forming fragments in the clot. The threshold value was calibrated based on experimental results according to the following workflow: first, a simulation of the tensile test up to a strain higher than the failure strain was run; then, the five highest PSMAX values in the clot at the failure strain were averaged to determine the threshold value (this had been done to avoid the influence of a local value which could be related to a single element); finally, the tensile test simulation was rerun using the calibrated failure model.

For comparing the stress-strain curve resulting from the simulation with the experimental stress-strain curve, considering the whole strain range covered in the experimental tests, an error was computed as:

$$err\% = \frac{\sqrt{\int_0^{\varepsilon_{max}} \left(\sigma_{exp} - \sigma_{comp}\right)^2 d\varepsilon}}{\sqrt{\int_0^{\varepsilon_{max}} \left(\sigma_{exp}\right)^2 d\varepsilon}} \times 100 \quad (1)$$

For compression the entire tested strain range (from 0 to −80%) was considered, while for tension the strain range up to the failure was considered.

2.2. Verification analysis of the failure criterion

Preliminary thrombectomy simulations showed an influence of the mesh size of the thrombus on the amount of volume which is cancelled from the calculation due to the failure criterion. The two steps of the simulation useful for studying this influence are the deployment and the retrieval, since the stent-retriever exerts a force on the thrombus. Thus, a simplified thrombectomy case was simulated considering only an idealized straight occlusion site (M1 tract of the Middle Cerebral Artery), where the thrombus was positioned. The same simulation settings that will be reported in section 2.3 were here used. The material model of the red thrombus obtained from replicating the experimental tests was assigned to the clot. The ET stent-retriever crimped in the microcatheter was placed across the occlusion (Fig. 3a) and deployed (Fig. 3b). Then, the stent-thrombus complex was retrieved to the end of the idealized M1 (Fig. 3c). Considering that the cross section of the stent-retriever beams was 0.075 mm of diameter (Fig. 3d), four mesh sizes were considered for discretizing the thrombus, going from 0.2 to 0.05 mm. For a better computation of the contact algorithms the elements of the thrombus and the elements of the stent-retriever should have similar dimensions, thus four simulations were run, changing the length of the beams of the stent-retriever according to the element size of the thrombus (Table 1).

All four simulations were run with the PSMAX threshold value of the failure criterion calibrated based on the experimental tensile test. For quantifying the fragmentation, the percentage of cancelled volume over the initial thrombus volume was computed. To do so the initial volume of each tetrahedron was saved along with the element identification number (ID). All volumes were summed to obtain the total initial volume. At selected timepoints of the simulation, the ID of each cancelled tetrahedron is saved and the volumes of all the cancelled tetrahedron are summed to obtain the total cancelled volume. The percent cancelled volume found with the finest mesh was set as target. Thus, a trial-and-error approach was used to find the PSMAX threshold value to be used with the coarser mesh (0.2 mm) in order to reach the target cancelled volume.

2.3. In silico thrombectomy procedure

Three stent-retriever models resembling three different design concepts were considered for this study (Fig. 4): EmboTrap II 5 × 33 (ET) (CERENOVUS, Galway, Ireland), Solitaire X 6 × 40 (SX) (Medtronic, USA), and Trevo ProVue 6 × 25 (TP) (Stryker, USA). ET has a dual-layer design, composed by an outer stent cage with large openings and leaflets, and an inner closed-cell stent. Differently from ET, SX is characterized by a single open structure, while TP has a single closed structure with open tails (Fig. 4). After a mesh sensitivity analysis, all stent-retrievers were discretized with beam elements of 0.2 mm of length. To the tip of all stents a 13 mm long wire, discretized with 0.2 mm beam elements, was attached.

A shape memory material model resembling Nitinol is assigned to the three stent-retrievers. The calibration of the Nitinol parameters for these stents and mesh sensitivity analysis can be found in (Luraghi et al., 2021a; Luraghi et al., 2022b).

An averaged patient anatomy (Fig. 5a) was created based on the results of Bridio et al. (2021); Bridio et al. (2023). In Bridio et al., 2021) 27 geometric parameters, including, among the others, the average diameters of the Anterior Cerebral Artery (ACA), and of the segments of the Middle Cerebral Artery (MCA, M1 and M2 segments), average diameters of the superior, anterior, posterior and inferior bends of the Internal Carotid Artery (ICA), as well as the angles formed at the T-junction and the M2 bifurcation, were identified. Then, in Bridio et al. (2023) 19 of these parameters were selected and changed to generate a virtual cohort of patients, starting from a training dataset of 88 cerebrovascular anatomies segmented from AIS patients' images. Here, the same process was used, with each of the 19 parameters taking the median values found in the training dataset to create an averaged patient model. For the simulation, the vessels were discretized with 0.3 mm rigid triangular elements.

The thrombus dimensions and location were taken from the literature to replicate the most common AIS event, visible in Fig. 5b. The thrombus was modelled as a cylinder of 13.5 mm of length, which was the median thrombus length found in Boodt et al. (2020) considering 367 AIS patients. The thrombus was then positioned in the distal M1, right upstream the T-junction, which was the most frequent occlusion location found in Dutra et al. (2019), for a cohort of 408 patients. The thrombus was discretized with 0.2 mm tetrahedral elements

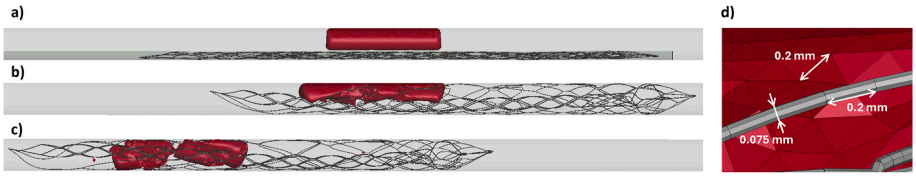

Fig. 3. Thrombectomy procedure in a simplified geometry. a) End of the tracking of the microcatheter with the crimped stent-retriever. b) End of the deployment of the stent-retriever. c) Retrieval. d) Thrombus mesh dimension compared to the beam length and diameter.

Table 1
Thrombus mesh sizes considered in the mesh sensitivity analysis, correspondent number of elements of the thrombus, and stent-retriever beam length for the correct computation of the contact algorithm.

Thrombus mesh size (mm)	Number of thrombus elements	Stent-retriever beam length (mm)
0.2	29968	0.2
0.1	228169	0.1
0.07	553959	0.05
0.05	1724161	0.05

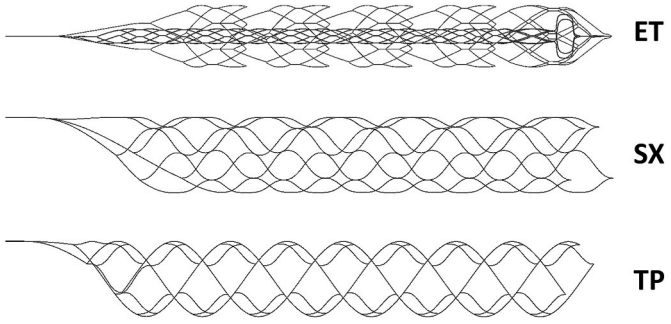

Fig. 4. Numerical models of the three devices considered in this work.

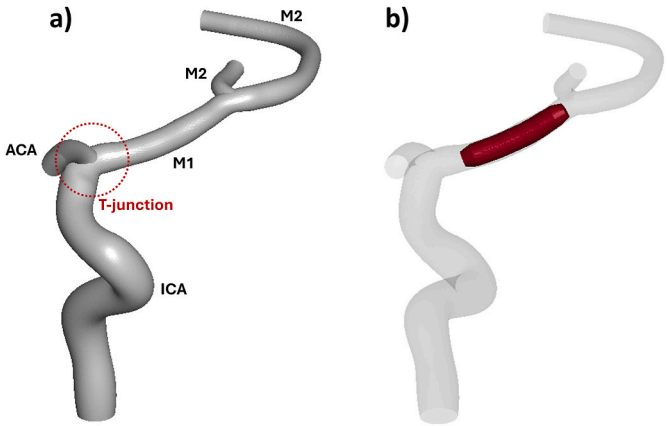

Fig. 5. a) Averaged patient's vessels b) Positioned thrombus.

(Fig. 6-magnification), which resulted the best compromise between computational time and cancelled thrombus volume in the simulation presented in section 2.2. The material model obtained replicating the experimental tests on human clot analogues was assigned to the thrombus, while the PSMAX threshold was adjusted to account for the effect of the mesh dimension, as explained in section 2.2.

A 0.8 mm microcatheter was modelled as a hollow cylindrical shell of length 130 mm and discretized with 0.15 mm orthogonal triangular elements (Fig. 6-magnification). This microcatheter was assigned a linear elastic material with an elastic modulus of 35 MPa, determined

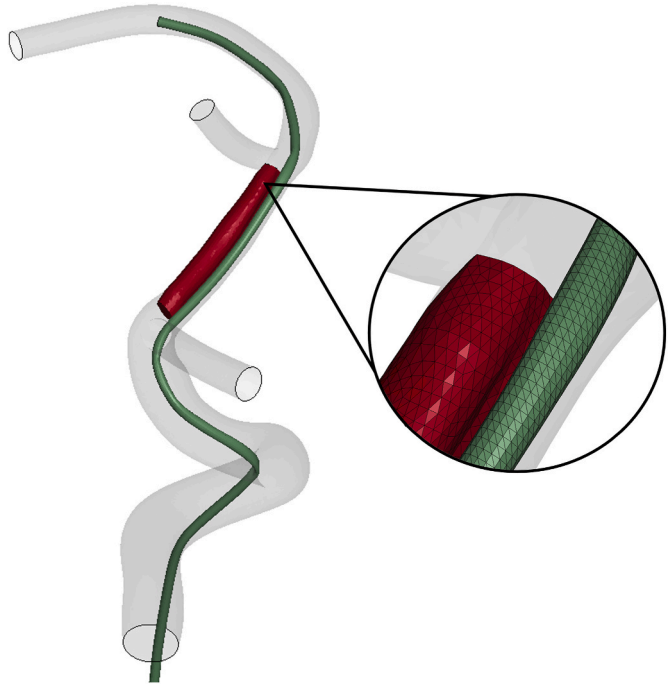

Fig. 6. Position of the microcatheter (green) at the end of the tracking step, with a magnification of the meshes of the thrombus and the microcatheter. The piece of rigid catheter pushing the clot against the wall is not shown. (For interpretation of the references to colour in this figure legend, the reader is referred to the Web version of this article.)

after a sensitivity analysis on the stiffness to have a reliable navigation, avoiding kinking. At the proximal end of the ICA a rigid 2.5 mm diameter aspiration catheter, modelled as a hollow cylindrical shell discretized with 1 mm quadrangular elements, was placed to collect stent-retriever and thrombus at the end of the retrieval.

The simulation of the EVT procedure consisted of four steps:

1. Stent crimping and thrombus positioning: the stent-retriever was crimped in the deformable microcatheter. A soft penalty contact was defined between the stent and the catheter. At the same time the thrombus was positioned at the distal M1 and pushed against the vessel wall by a piece of rigid catheter. A soft penalty contact with a static friction coefficient of 0.2 (Gunning et al., 2018) was set between thrombus and vessel;
2. Microcatheter tracking: the microcatheter tip was moved following the centreline of the vessels, while the microcatheter body could adjust itself, better resembling clinical scenarios with respect to the previous method where the entire catheter was constrained to remain on the centreline (Arrarte Terreros et al., 2023). Near the thrombus, the centreline was modified so that the microcatheter could pass on one side of the thrombus, as shown in Fig. 6. A soft penalty contact with a static friction coefficient of 0.5 and a dynamic friction coefficient of 0.4 was defined between stent and microcatheter so that moving the catheter, the crimped stent was dragged.

A soft penalty contact without friction was defined between thrombus and microcatheter;
3. Deployment: the stent was released by sliding the microcatheter from the stent, coming in contact with vessel and thrombus. A soft penalty contact was defined between stent and vessel, and stent and thrombus (with a static friction coefficient of 0.2 and a dynamic friction coefficient of 0.15);
4. Retrieval: the stent, with the entrapped thrombus, was retrieved by pulling the end of the wire until the stent was re-crimped inside the aspiration catheter.

All meshes were created in ANSA, and all the simulations were run using the commercial explicit finite-element solver LS-DYNA R14 with 28 CPUs (Intel Xeon64) and 250 GB of RAM memory. Mass proportional dampings were adopted: 1 s^{-1} for the thrombus, 10 s^{-1} for the stent and the microcatheter in order to improve stability (Luraghi et al., 2018). A selective mass scaling was used to use a constant timestep of 10^{-6} s to speed up the computation as recommended by the LS-DYNA Support (https://www.dynasupport.com/howtos/general/quasistatic-simulation). The real timings of the procedure were scaled down to reduce the computational time. However, to do that with an explicit time integration the loads should be slow enough to be in a quasi-static condition, to minimize the inertia effects. In all simulations it was verified that the ratio between the kinetic and the internal energy was less than 5%.

For each thrombus composition, three stent-retriever models were considered, resulting in a total of nine simulations. For the analysis of the results of the EVT simulations, a qualitative comparison among the nine combinations is performed in terms of deformation and fragmentation of the thrombus, and success of the retrieval. To quantify the fragmentation, the percentage of the cancelled thrombus volume relative to the initial thrombus volume is computed, as an index of the force which is exerted to the thrombus by the stent-retriever.

3. Results

3.1. Clot modelling

3.1.1. Experimental characterisation of clot analogues

The results of the compression and tensile tests are reported in Fig. 7. In compression the clot analogues of all three compositions exhibited a non-linear stress-strain behaviour, with an increase of the stiffness with increasing strain. There was negligible difference between 0% and 1% RBCs curves (stress at 0.8 strain: 67 kPa, and −69 kPa, respectively), while the 40% RBCs sample showed a much lower stiffness and stress at 0.8 strain (−3.7 kPa). Differently from compression, the tensile curves showed an almost linear behaviour. The 0% RBCs sample had the highest stiffness, closely followed by the 1% RBCs, while the 40% RBCs was far less stiff than the others. 0% and 1% RBCs fractured approximately at the same strain (1.21 and 1.20 strain, respectively), but with different stresses (68.6 kPa, and 52 kPa, respectively). The 40% RBCs sample fractured at a lower strain, with a much smaller stress (0.94 strain, 2.9 kPa). In all cases the fracture of the sample was almost instantaneous.

The estimation of the Poisson's ratio from the pictures taken during the tensile test resulted in an average value of 0.3.

3.1.2. In silico replica of the experimental test

The stress-strain curves resulting from the *in silico* replica of the experimental tests are compared with the experimental ones in Fig. 8. The errors computed with Equation (1) are reported in Table 2 along with the correspondent coefficients of determination R^2.

The PSMAX thresholds calibrated based on the experimental curves were 0.1434 MPa, 0.1193 MPa, and 0.00862 MPa for the 0% RBCs, 1% RBCs and 40% RBCs, respectively.

3.2. Verification analysis of the failure criterion

The results of the mesh sensitivity analysis are reported in Table 3. In Fig. 9 the red thrombus and stent are showed at the end of the deployment in the four cases considered. When the dimension of the thrombus elements was 0.2 mm or 0.1 mm, thus larger than the diameter of the cross section of the stent elements (0.075 mm), the stress distribution was similar. Consequently, these two cases did not display a sensible difference in terms of cancelled volume at the end of the stent-retriever deployment. With the thrombus discretized with 0.05 mm tetrahedral elements the cancelled volume approximately halved with respect to the coarser mesh. This is due to the more local interaction between the stent struts and the thrombus, as visible in Fig. 10, where the comparison between the distributions of the PSMAX in the 0.2 mm and 0.05 mm case is shown. In the 0.05 mm case, the more local distribution allowed the penetration of the stent struts in the thrombus (Fig. 9e) without losing a high amount of volume (Fig. 10c).

Despite the more detailed results in terms of stent-thrombus interaction, the 0.05 mm mesh was not chosen for the EVT simulation in the cerebral vessels due to the too high computational cost. For obtaining 9% of cancelled volume with the 0.2 mm mesh, the PSMAX threshold was increased by 60%.

In Fig. 11 the stent-thrombus configuration obtained with the 0.2 mm mesh with the adjusted threshold and the 0.05 mm mesh is shown. Comparing the two results at the end of the deployment (Fig. 11 a1 and b1), and then during the retrieval (Fig. 11 a2 and b2) a visible difference is that with the coarser mesh (Fig. 11 a1 and a2) the thrombus was more

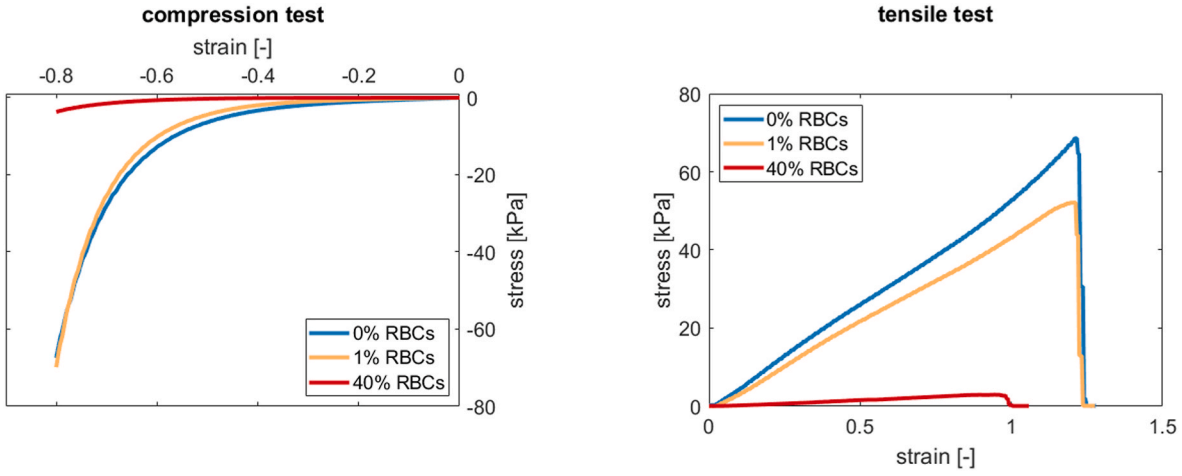

Fig. 7. Experimental stress-strain curves resulting from the compression and the tensile test for the three compositions.

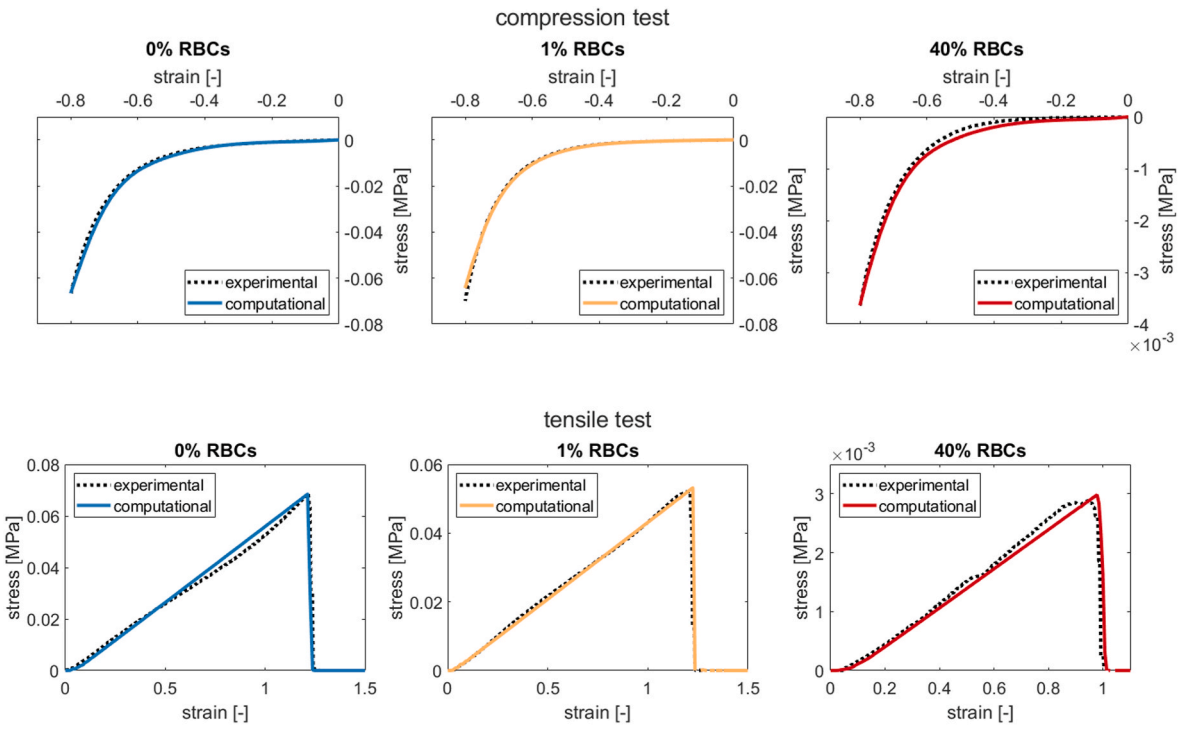

Fig. 8. Comparison of the stress-strain curves resulting from the simulations with the respective experimental stress-strain curves.

Table 2
Errors made by the computational stress-strain curve with respect to the experimental stress-strain curve.

Test	Composition	Error	R^2
Compression	0% RBCs	5.3%	0.996
	1% RBCs	4.1%	0.996
	40% RBCs	9.3%	0.990
Tensile	0% RBCs	5.2%	0.989
	1% RBCs	1.9%	0.996
	40% RBCs	5.4%	0.990

Table 3
Thrombus mesh sizes considered in the mesh sensitivity analysis with the correspondent cancelled volume and computational times.

Thrombus mesh size (mm)	Cancelled volume	Computational time
0.2	27%	5 h 27 min
0.1	17%	17 h 56 min
0.07	12%	29 h 11 min
0.05	9%	46 h 4 min

compressed against the vessel wall, while with the finest mesh (Fig. 11 b1 and b2), the stent struts penetrated the clot.

3.3. *In silico thrombectomy simulations*

The comparison among devices and thrombus compositions at the end of the deployment is reported in Fig. 12. In this simulation instant the stent-retriever, positioned across the thrombus, had been opened, and the thrombus was deformed and pushed against the vessel wall. Considering all nine cases, the volume cancelled from the simulation is 2% at most (red thrombus with SX model).

In Fig. 13 there is the comparison among devices and thrombus compositions at three different instants of the retrieval phase. With all three stent-retrievers the red thrombus fragmented, especially using the ET device, as visible also in Fig. 14, where the percentage of cancelled volume is plotted over time. The first sudden increase of volume which was cancelled from the simulation was in correspondence of the start of the pulling of the stent-retriever. Then, the other increases were in correspondence of the bends of the ICA, when the thrombus was pushed against the walls. In case of SX and TP devices, with a smaller cancelled volume, the fragments were bigger than the ones generated by ET, and some of them were lost at the end of the retrieval phase. The

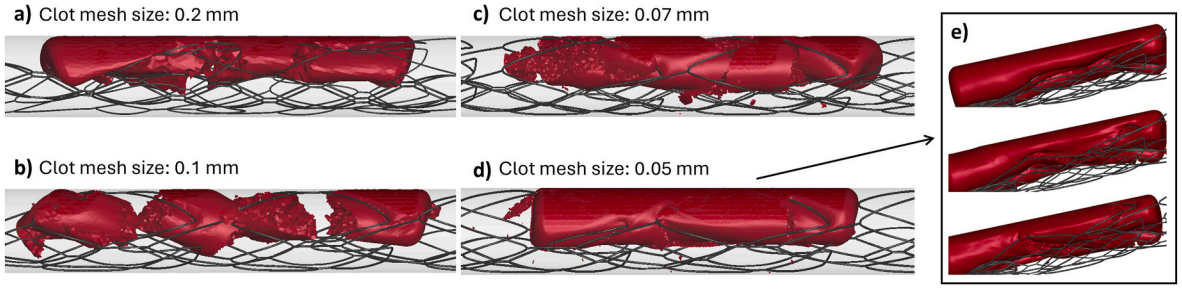

Fig. 9. Comparison of the stent-thrombus configuration at the end of the deployment among the different mesh sizes: a) mesh size 0.2 mm b) mesh size 0.1 mm c) mesh size 0.07 mm d) mesh size 0.05 mm. e) close up on the contact between stent-retriever and thrombus with mesh size 0.05 mm: the thrombus was firstly deformed and then penetrated by the stent struts.

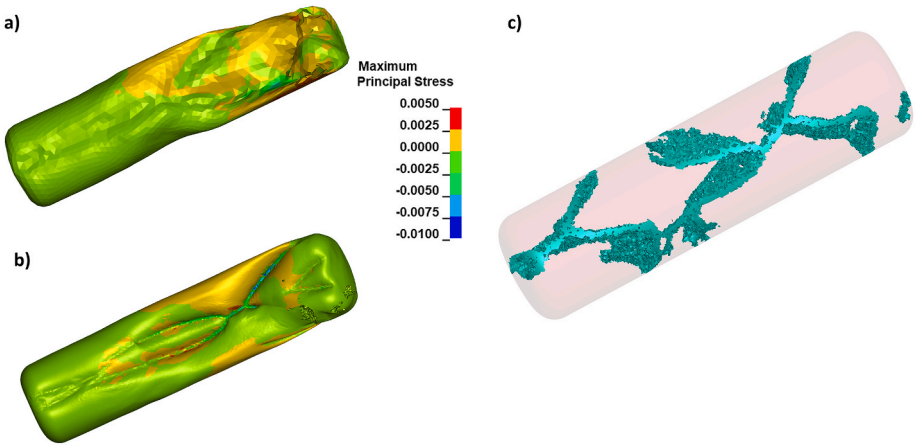

Fig. 10. PSMAX distribution on the surface of the thrombus in contact with the stent-retriever: a) mesh size 0.2 mm b) mesh size 0.05 mm. c) highlighted cancelled elements at the end of the deployment with the 0.05 mm mesh.

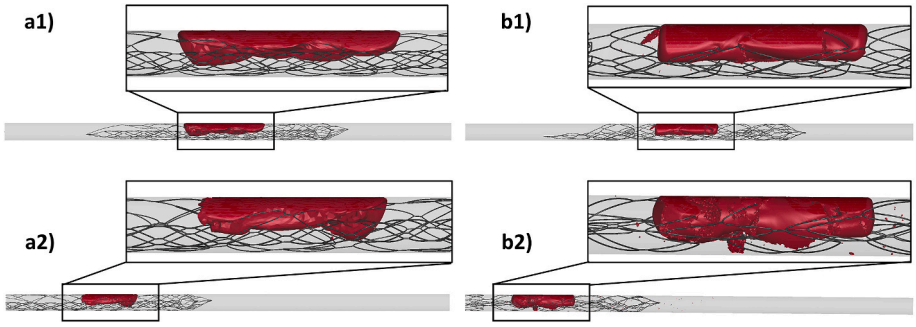

Fig. 11. Comparison of the two simulations with the same cancelled volume: a) stent-thrombus configuration with the 0.2 mm mesh and the adjusted threshold at the end of the deployment (a1) and during the retrieval (a2); b) stent-thrombus configuration with the 0.05 mm mesh at the end of the deployment (b1) and during the retrieval (b2).

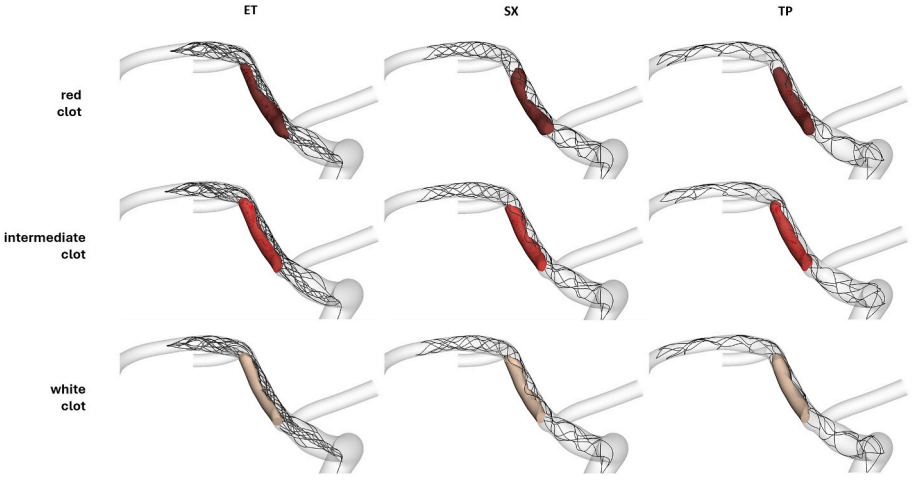

Fig. 12. Comparison among the different stent-thrombus configurations obtained at the end of the deployment with different thrombus composition and device (ET: Embotrap II; SX: Solitaire X; TP: Trevo ProVue).

intermediate and the white thrombi did not produce fragments, indeed the very small percentages of cancelled volume observed in these six cases (Table 4) were not enough to create a total discontinuity in the thrombi. A graphical representation of the decrease of cancelled volume with decreasing RBCs content for each stent-retriever model is shown in Fig. 15. Even though the fragmentation was low, in half of the cases intermediate and white thrombi were not successfully retrieved.

4. Discussion

Numerical models of clinical procedures have become a widespread technique for the study of the performance of the devices and their interaction with surrounding tissues and biological structures. In this view, our group proved the credibility of the thrombectomy FE simulations with stent-retriever (Luraghi et al., 2021c). The thrombus is a

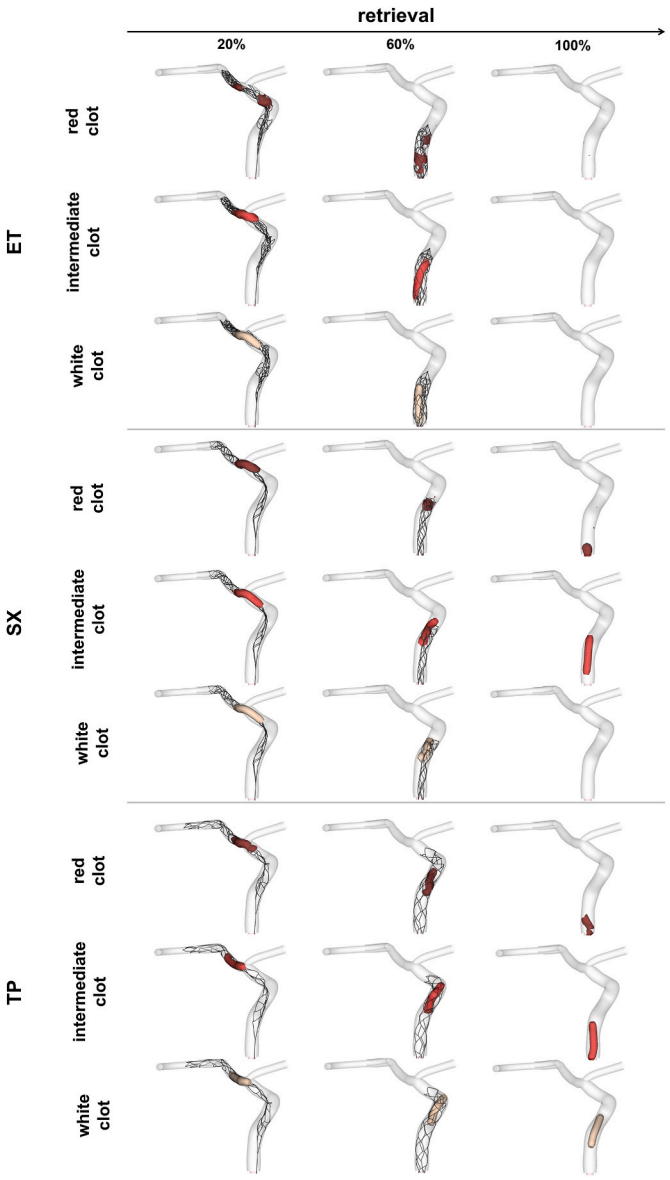

Fig. 13. Comparison among the results with different thrombus composition and device at three instants of the retrieval step.

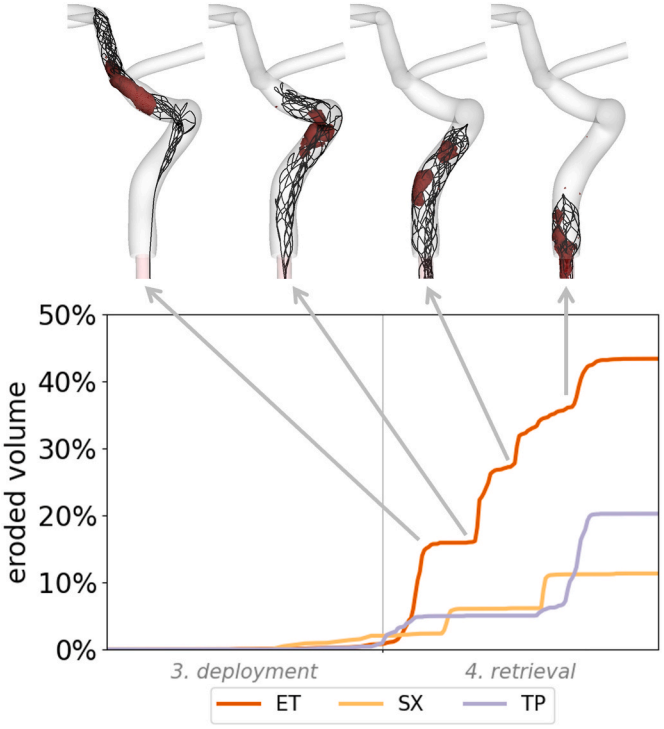

Fig. 14. Progression of the cancelled volume during the deployment and the retrieval steps of the simulation with the three different stent-retrievers used to retrieve the red thrombus. For ET four instants of the simulation are reported in correspondence to the sudden increases of the cancelled volume. (For interpretation of the references to colour in this figure legend, the reader is referred to the Web version of this article.)

Table 4
Volume which is cancelled from the simulation at the end of the retrieval for the nine combinations of stent-retrievers and thrombus compositions.

Stent-retriever	Cancelled volume at the end of retrieval		
	Red thrombus	Intermediate thrombus	White thrombus
ET	43.37%	0.72%	0.14%
SX	11.32%	0.07%	0.16%
TP	20.25%	0.00%	0.08%

crucial element in the procedure, and its fragmentation, which can cause distal embolism, is a challenge in the *in vivo* EVT procedure (Gascou et al., 2014; Chueh et al., 2016). Consequently, the accurate modelling of the thrombus in the *in silico* EVT is crucial. To achieve that, its mechanical properties should be studied and numerically replicated, considering their variability with thrombus composition and the significant tension-compression asymmetry (Cahalane et al., 2023), and including the possibility of thrombus fragmentation in the simulations.

The results of the compression test here performed were in line with the results found in the literature for human clot analogues (Cahalane et al., 2023; Cruts et al., 2023). Similar results were found for animal clot analogues (Liang et al., 2017; Chueh et al., 2011; Fereidoonnezhad et al., 2021a,b; Johnson et al., 2020; Malone et al., 2018), and for retrieved thrombi (Boodt et al., 2021). Moreover, as previously found by Cahalane et al. (2023); Cruts et al. (2023) with the same experimental protocol here followed and by Liang et al. (2017); Boodt et al. (2021), here it was found that the increase in RBCs content was associated to a decrease of the stiffness. This was especially true when comparing RBCs-poor (0% RBCs and 1% RBCs) and RBCs-rich (40% RBCs) clots. Confirming the results of Cahalane et al. (2023), under tensile loading an almost linear stress-strain behaviour was observed. Again, an increase in RBCs content (in the blood mixture) from 0% to 40% was linked to a decrease in stiffness as in Liu et al. (2020); Cahalane et al. (2023). Confirming again the results of Cahalane et al. (2023), considering compression and tension together a significant tension-compression asymmetry was found, underling the importance of considering both loading types for the characterisation of clot analogues and the definition of a material model suitable for numerical simulations. From the pictures of the samples subjected to tensile test, a Poisson's ratio of 0.3 was estimated, which is in line with the choice previously made by Luraghi et al., 2021a). With respect to previous works made with the same experimental protocol, in the present work, particular attention has been put to the accurate recording of the shape of the experimental samples by means of pictures and ultrasound images, in order to be able to replicate it in the CAD models. Having *in silico* geometries resembling as much as possible the experimental ones is fundamental for the correct calibration of the material model.

The mechanical behaviour of the clot was modelled using a tabulated model implemented in LS-DYNA and based on the work by Kolling et al. (2007). The model can accommodate non-linear elastic behaviour, but also realistic unloading behaviour with energy dissipation, based on user

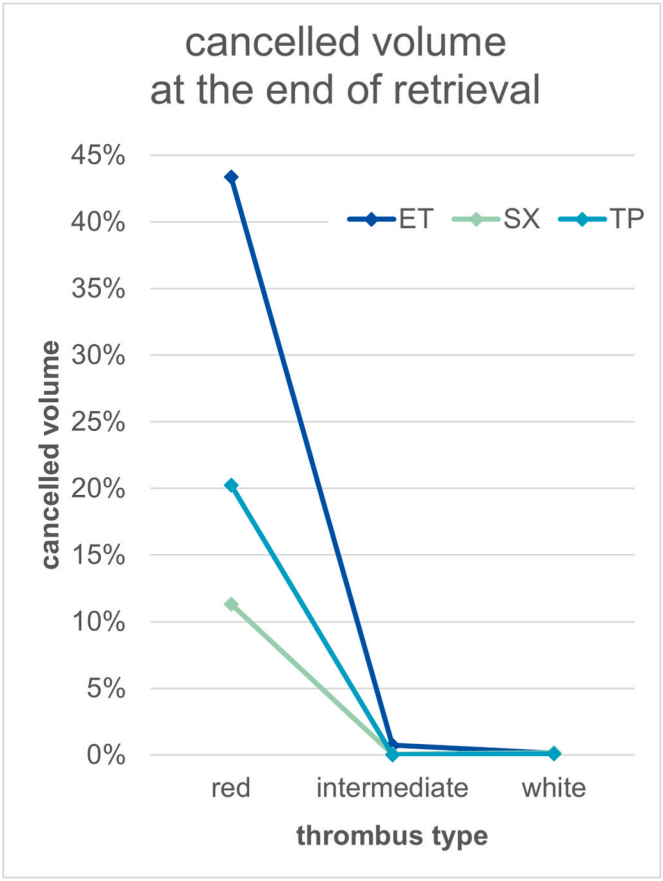

Fig. 15. Cancelled thrombus volume trend with decreasing RBCs content for each stent-retriever model.

input of uniaxial stress-strain data. In this regard, we have decided to use the model limited to a non-linear elastic case as described in Appendix B. With errors between experimental and computational stress-strain curves under 10%, the tabulated material model here used proved capable of replicating the asymmetry of the stress-strain curve in both tension and compression. The advantage of this material model is that no time-consuming fitting operation is needed to determine the hyperelastic coefficients as required in the classical analytical formulations, since it requires only uniaxial test data, without needing any other type of mechanical test. Moreover, it could meet the need of describing a compressible hyperelastic material with the addition of stress-strain curve asymmetry in compression and tension. The decision to neglect the rate dependency of thrombus mechanical behaviour is based on the assumption that virtual EVT takes place sufficiently fast as to minimize viscoelastic effects.

Additionally, the use of a failure criterion based on a PSMAX threshold led to an instantaneous fracture of the samples, as in the experimental tensile tests. This happened because the elements constituting the most loaded section of the clot overcome the PSMAX threshold almost at the same time: when the first elements were cancelled, the resistant section decreased, and the remaining elements rapidly overcome the threshold. Thus, in very few timesteps, all the elements constituting that section were cancelled, and a complete discontinuity in the thrombus was created. As a consequence, this material model, for the first time based on human data, was deemed suitable for its use in EVT simulations. However, the failure of the clot analogue during tensile testing and the fragmentation of the thrombus during the EVT have slightly different mechanisms. In the latter, indeed, the fragmentation of the thrombus was mainly due to the stresses generated by the interaction between the thrombus and the stent-retriever, which pushed the thrombus against the vessel wall. The distribution of the stresses was dependent on the mesh size of the thrombus with respect to the diameter of the stent-retriever struts. Consequently, also the cancelled volume was dependent on the thrombus mesh size. Reducing the thrombus mesh size the cancelled volume converged, but the computational cost of the simulation was not acceptable. The use of a coarser mesh with an adjustment of the PSMAX threshold to address this numerical problem was preferred. In the simplified M1 geometry, the comparison between the two configurations (0.2 mm and 0.05 mm mesh) with equal cancelled volume showed a different behaviour in the interaction between thrombus and stent. With the coarser mesh, indeed, the stent pushed the thrombus against the vessel wall, deforming it, while with the finest mesh the stent-struts could penetrate in the thrombus. However, the two configurations were similar in terms of quantity of fragments that were produced, since in both cases the thrombus was still a single piece.

For the *in silico* procedure, nine FE simulations were carried out using combinations of three thrombus compositions and three stent-retriever models. The selection of three stent-retriever models was made to assess whether the thrombus behaviour, such as fragmentation, could be affected by the stent-retriever design. This work is a proof-of-concept towards clinical applications and the results are discussed according to the specific modelled procedure: using a stent-retriever alone, without an aspiration catheter, assuming flow arrest due to the presence of a ballon guide catheter, and having calibrated the material model based on data from a single donor. The outcomes of the simulations by changing the thrombus mechanical properties were in line with the literature regarding the different proneness to fragmentation of thrombi with different compositions (Kaesmacher et al., 2017; Fereidoonnezhad et al., 2021a,b). In particular, RBCs-rich (red) thrombi also in this work seemed to be more prone to fragmentation than RBCs-poor (intermediate and white) thrombi. Indeed, the cancelled volume with respect to the initial thrombus volume in case of red thrombi spanned from 11% to more than 40%, meaning that a non-negligible number of elements overcame the PSMAX threshold, leading to the formation of fragments. Instead, intermediate and white thrombi did not produce fragments, and in general seemed to be more difficult to be retrieved since they were pushed against the vessel wall, while being less engaged in the stent struts, as observed also experimentally in (Machi et al., 2017). The differences in thrombus behaviour using three different stent-retrievers could be due to their different design, which led to a different radial force, different distribution of the points of contact with the thrombus, and consequently different distribution of the stresses in the thrombus. For example, the high cancelled volume of the red thrombus retrieved with ET model could be due to the double metallic structure, which came in contact with a greater number of elements with respect to the single metallic structure of SX and TP models.

This work has limitations. First, for the mechanical characterisation of the clot analogues, blood was drawn from only one donor, and only one sample for each composition and type of test has been considered. A larger number of samples also from different donors should be included in the future to contrast possible variabilities due to test and donor. In addition, in the tests only the loading was performed; considering both loading and unloading could provide a complete characterisation, allowing a more realistic behaviour of the thrombus in the virtual retrieval phase, where the stresses in the clot not necessarily are monotonically increasing. Moreover, in the virtual procedure, while changing thrombus composition, the choice to keep the friction coefficient constant between the thrombi and the vessel wall, as well as between the thrombi and the device, was made because: i) we intentionally changed only the thrombus mechanical properties in the simulations, keeping all other settings the same to avoid introducing confounding variables and to compare the outcomes by studying only the impact of thrombus compositions; ii) there is a lack of detailed and consistent values in the literature. In reality, however, a different thrombus composition in terms of RBCs content would lead to a different friction

coefficient. In particular, friction coefficient quantifications performed on clot analogues made from animal blood (ovine in Gunning et al., 2018 and bovine in Elkhayyat et al., 2024) tested on different materials (PTFE in Gunning et al., 2018, silicone, glass, and PVC Elkhayyat et al., 2024, and bovine arterial tissue in both Gunning et al., 2018; Elkhayyat et al., 2024) showed that the static friction coefficient decreased with increasing RBCs content. As a consequence, here, the difficulty in retrieving RBCs-poor thrombi would probably be increased with respect to the presented results. Third, the vessel wall was modelled with a rigid material. The influence of vessel wall elasticity on the outcome of the EVT should be investigated in future studies. Then, the presence of blood was neglected because it would have required a fluid-structure interaction simulation, which is very costly. This implies that the thrombus has no residual stresses from blood pressure before the EVT procedure. Lastly, the failure model here used implied the loss of thrombus volume during the virtual EVT procedure, thus, in the future, an improvement of the failure model should be made, validating with specific *in vitro* evidence.

5. Conclusions

In this work, an experimental characterisation of human clot analogues with different compositions was conducted to calibrate a material model, incorporating failure, for use in finite element simulations of EVT. The resulting stress-strain curves revealed compression-tension asymmetry and instantaneous fracture of the clot analogues under tension. This experimental behaviour was replicated *in silico*. The effect of the adopted failure criterion, based on setting a PSMAX threshold, was found to be dependent on the thrombus mesh size in the EVT procedure, due to contact with the stent retriever. A converging trend in the cancelled volume, caused by the failure, was observed as the thrombus mesh size decreased. However, decreasing the mesh size increased the computational cost. Therefore, to contain computational costs, the PSMAX threshold was adjusted to achieve with the coarsest mesh the same cancelled volume achieved with the finest mesh. Finally, nine EVT simulations were performed, varying clot composition and stent-retriever design. These simulations demonstrated a greater proneness to fragmentation in RBC-rich thrombi compared to RBC-poor thrombi and highlighted the influence of stent-retriever design on the outcome of the *in silico* procedure.

CRediT authorship contribution statement

Virginia Fregona: Writing – original draft, Methodology, Investigation, Conceptualization. **Giulia Luraghi:** Writing – review & editing, Methodology, Conceptualization. **Behrooz Fereidoonnezhad:** Writing – review & editing, Investigation, Data curation. **Frank J.H. Gijsen:** Writing – review & editing, Supervision, Methodology, Conceptualization. **Charles B.L.M. Majoie:** Writing – review & editing, Funding acquisition. **Jose Felix Rodríguez Matas:** Writing – review & editing, Methodology, Conceptualization. **Francesco Migliavacca:** Writing – review & editing, Supervision, Funding acquisition.

Funding

GEMINI has received funding from the European Union's Horizon 2020 research and innovation programme under the grant agreement No 101136438.

Declaration of competing interest

The authors declare the following financial interests/personal relationships which may be considered as potential competing interests: All authors report financial support was provided by European Union's Horizon 2020. Charles B.L.M. Majoie reports a relationship with Boeringher-Ingelheim that includes: funding grants. Charles B.L.M. Majoie reports a relationship with Stryker that includes: consulting or advisory. Charles B.L.M. Majoie reports a relationship with Nico.lab that includes: equity or stocks. If there are other authors, they declare that they have no known competing financial interests or personal relationships that could have appeared to influence the work reported in this paper.

Appendix A-C. Supplementary data

Supplementary data to this article can be found online at https://doi.org/10.1016/j.jmbbm.2025.106886.

Data availability

Data will be made available on request.

References

Abbafati, C., Abbas, K.M., Abbasi-Kangevari, M., Abd-Allah, F., Abdelalim, A., Abdollahi, M., Abdollahpour, I., Abegaz, K.H., Abolhassani, H., Aboyans, V., Abreu, L.G., Abrigo, M.R.M., Abualhasan, A., Abu-Raddad, L.J., Abushouk, A.I., Adabi, M., Adekanmbi, V., Adeoye, A.M., Adetokunboh, O.O., et al., 2020. Global burden of 369 diseases and injuries in 204 countries and territories, 1990–2019: a systematic analysis for the Global Burden of Disease Study 2019. Lancet 396 (10258), 1204–1222. https://doi.org/10.1016/S0140-6736(20)30925-9.

Arrarte Terreros, N., Renon, S., Zucchelli, F., Bridio, S., Rodriguez Matas, J.F., Dubini, G., Konduri, P.R., Koopman, M.S., van Zwam, W.H., Yo, L.S.F., Lo, R.H., Marquering, H. A., van Bavel, E., Majoie, C.B.L.M., Migliavacca, F., Luraghi, G., 2023. Microcatheter tracking in thrombectomy procedures: a finite-element simulation study. Comput. Methods Progr. Biomed. 234, 107515. https://doi.org/10.1016/j.cmpb.2023.107515.

Berkhemer, O.A., Fransen, P.S.S., Beumer, D., van den Berg, L.A., Lingsma, H.F., Yoo, A. J., Schonewille, W.J., Vos, J.A., Nederkoorn, P.J., Wermer, M.J.H., van Walderveen, M.A.A., Staals, J., Hofmeijer, J., van Oostayen, J.A., Lycklama à Nijeholt, G.J., Boiten, J., Brouwer, P.A., Emmer, B.J., de Bruijn, S.F., et al., 2015. A randomized trial of intraarterial treatment for acute ischemic stroke. N. Engl. J. Med. 372 (1), 11–20. https://doi.org/10.1056/nejmoa1411587.

Boeckh-Behrens, T., Schubert, M., Förschler, A., Prothmann, S., Kreiser, K., Zimmer, C., Riegger, J., Bauer, J., Neff, F., Kehl, V., Pelisek, J., Schirmer, L., Mehr, M., Poppert, H., 2016. The impact of histological clot composition in embolic stroke. Clin. Neuroradiol. 26 (2), 189–197. https://doi.org/10.1007/s00062-014-0347-x.

Boodt, N., Compagne, K.C.J., Dutra, B.G., Samuels, N., Tolhuisen, M.L., Alves, H.C.B.R., Kappelhof, M., Lycklama À Nijeholt, G.J., Marquering, H.A., Majoie, C.B.L.M., Lingsma, H.F., Dippel, D.W.J., Van Der Lugt, A., 2020. Stroke etiology and thrombus computed tomography characteristics in patients with acute ischemic stroke: a mr clean registry substudy. Stroke 51 (6), 1727–1735. https://doi.org/10.1161/STROKEAHA.119.027749.

Boodt, N., Snouckaert Van Schauburg, P.R.W., Hund, H.M., Fereidoonnezhad, B., McGarry, J.P., Akyildiz, A.C., Van Es, A.C.G.M., De Meyer, S.F., Dippel, D.W.J., Lingsma, H.F., Van Beusekom, H.M.M., Van Der Lugt, A., Gijsen, F.J.H., 2021. Mechanical characterization of thrombi retrieved with endovascular thrombectomy in patients with acute ischemic stroke. Stroke 2510–2517. https://doi.org/10.1161/STROKEAHA.120.033527. August.

Bridio, S., Luraghi, G., Ramella, A., Rodriguez Matas, J.F., Dubini, G., Luisi, C.A., Neidlin, M., Konduri, P., Arrarte Terreros, N., Marquering, H.A., Majoie, C.B.L.M., Migliavacca, F., 2023. Generation of a virtual cohort of patients for in silico trials of acute ischemic stroke treatments. Appl. Sci. 13 (18). https://doi.org/10.3390/app131810074.

Bridio, S., Luraghi, G., Rodriguez Matas, J.F., Dubini, G., Giassi, G.G., Maggio, G., Kawamoto, J.N., Moerman, K.M., McGarry, P., Konduri, P.R., Arrarte Terreros, N., Marquering, H.A., van Bavel, E., Majoie, C.B.L.M., Migliavacca, F., 2021. Impact of the internal Carotid artery morphology on in silico stent-retriever thrombectomy outcome. Front. Med. Technol. 3 (August), 1–13. https://doi.org/10.3389/fmedt.2021.719909.

Cahalane, R., Boodt, N., Akyildiz, A.C., Giezen, J.-A., Mondeel, M., van der Lugt, A., Marquering, H., Gijsen, F., 2021. A review on the association of thrombus composition with mechanical and radiological imaging characteristics in acute ischemic stroke. J. Biomech. 129 (October), 110816. https://doi.org/10.1016/j.jbiomech.2021.110816.

Cahalane, R.M.E., Cruts, J.M.H., Beusekom, H. M. M. Van, Maat, M.P. M. De., 2024. Contribution of red blood cells and platelets to blood clot computed tomography imaging and compressive mechanical characteristics. Ann. Biomed. Eng. https://doi.org/10.1007/s10439-024-03515-y.

Cahalane, R.M.E., de Vries, J.J., de Maat, M.P.M., van Gaalen, K., van Beusekom, H.M., van der Lugt, A., Fereidoonnezhad, B., Akyildiz, A.C., Gijsen, F.J.H., 2023. Tensile and compressive mechanical behaviour of human blood clot analogues. Ann. Biomed. Eng., 0123456789 https://doi.org/10.1007/s10439-023-03181-6.

Chalumeau, V., Blanc, R., Redjem, H., Ciccio, G., Smajda, S., Desilles, J.-P., Botta, D., Escalard, S., Boisseau, W., Maïer, B., Labreuche, J., Obadia, M., Piotin, M., Mazighi, M., 2018. Anterior cerebral artery embolism during thrombectomy

increases disability and mortality. J. Neurointerventional Surg. 10 (11). https://doi.org/10.1136/neurintsurg-2018-013793, 1057 LP – 1062.
Chueh, J.Y., Puri, A.S., Wakhloo, A.K., Gounis, M.J., 2016. Risk of distal embolization with stent retriever thrombectomy and ADAPT. J. Neurointerventional Surg. 8 (2), 197–202. https://doi.org/10.1136/neurintsurg-2014-011491.
Chueh, J.Y., Wakhloo, A.K., Hendricks, G.H., Silva, C.F., Weaver, J.P., Gounis, M.J., 2011. Mechanical characterization of thromboemboli in acute ischemic stroke and laboratory embolus analogs. Am. J. Neuroradiol. 32 (7), 1237–1244. https://doi.org/10.3174/ajnr.A2485.
Chugh, C., 2019. Acute ischemic stroke: management approach. Indian J. Crit. Care Med. 23, S140–S146. https://doi.org/10.5005/jp-journals-10071-23192.
Cines, D.B., Lebedeva, T., Nagaswami, C., Hayes, V., Massefski, W., Litvinov, R.I., Rauova, L., Lowery, T.J., Weisel, J.W., 2014. Clot contraction: compression of erythrocytes into tightly packed polyhedra and redistribution of platelets and fibrin. Blood 123 (10), 1596–1603. https://doi.org/10.1182/blood-2013-08-523860.
Cruts, J.M.H., Giezen, J.A., van Gaalen, K., Beurskens, R., Ridwan, Y., Dijkshoorn, M.L., van Beusekom, H.M.M., Boodt, N., van der Lugt, A., de Vries, J.J., de Maat, M.P.M., Gijsen, F.J.H., Cahalane, R.M.E., 2023. The association between human blood clot analogue computed tomography imaging, composition, contraction, and mechanical characteristics. PLoS One 18 (11 NOVEMBER), 1–15. https://doi.org/10.1371/journal.pone.0293456.
Dutra, B.G., Tolhuisen, M.L., Alves, H.C.B.R., Treurniet, K.M., Kappelhof, M., Yoo, A.J., Jansen, I.G.H., Dippel, D.W.J., Van Zwam, W.H., Van Oostenbrugge, R.J., Da Rocha, A.J., Lingsma, H.F., Van Der Lugt, A., Roos, Y.B.W.E.M., Marquering, H.A., Majoie, C.B.L.M., 2019. Thrombus imaging characteristics and outcomes in acute ischemic stroke patients undergoing endovascular treatment. Stroke 50 (8), 2057–2064. https://doi.org/10.1161/STROKEAHA.118.024247.
Elkhayyat, O.N., Froehler, M.T., Good, B.C., 2024. Analysis of frictional forces in experimental models of stent retriever mechanical thrombectomy. J. Biomech. 164 (January), 1–6. https://doi.org/10.1016/j.jbiomech.2024.111971.
Feigin, V.L., Abate, M.D., Abate, Y.H., Abd ElHafeez, S., Abd-Allah, F., Abdelalim, A., Abdelkader, A., Abdelmasseh, M., Abd-Elsalam, S., Abdi, P., Abdollahi, A., Abdoun, M., Abd-Rabu, R., Abdulah, D.M., Abdullahi, A., Abebe, M., Abeldaño Zuñiga, R.A., Abhilash, E.S., Abiodun, O.O., Murray, C.J.L., 2024a. Global, regional, and national burden of stroke and its risk factors, 1990–2021: a systematic analysis for the Global Burden of Disease Study 2021. Lancet Neurol. 23 (10), 973–1003. https://doi.org/10.1016/S1474-4422(24)00369-7.
Feigin, V.L., Abate, M.D., Abate, Y.H., Abd ElHafeez, S., Abd-Allah, F., Abdelalim, A., Abdelkader, A., Abdelmasseh, M., Abd-Elsalam, S., Abdi, P., Abdollahi, A., Abdoun, M., Abd-Rabu, R., Abdulah, D.M., Abdullahi, A., Abebe, M., Abeldaño Zuñiga, R.A., Abhilash, E.S., Abiodun, O.O., Murray, C.J.L., 2024b. Global, regional, and national burden of stroke and its risk factors, 1990–2021: a systematic analysis for the Global Burden of Disease Study 2021. Lancet Neurol. 23 (10), 973–1003. https://doi.org/10.1016/S1474-4422(24)00369-7.
Fereidoonnezhad, B., Dwivedi, A., Johnson, S., McCarthy, R., McGarry, P., 2021a. Blood clot fracture properties are dependent on red blood cell and fibrin content. Acta Biomater. 127, 213–228. https://doi.org/10.1016/j.actbio.2021.03.052.
Fereidoonnezhad, B., Moerman, K.M., Johnson, S., McCarthy, R., McGarry, P.J., 2021b. A new compressible hyperelastic model for the multi-axial deformation of blood clot occlusions in vessels. Biomech. Model. Mechanobiol. 20 (4), 1317–1335. https://doi.org/10.1007/s10237-021-01446-4.
Gascou, G., Lobotesis, K., Machi, P., Maldonado, I., Vendrell, J.F., Riquelme, C., Eker, O., Mercier, G., Mourand, I., Arquizan, C., Bonafé, A., Costalat, V., 2014. Stent retrievers in acute ischemic stroke: complications and failures during the perioperative period. Am. J. Neuroradiol. 35 (4), 734–740. https://doi.org/10.3174/ajnr.A3746.
Goyal, M., Demchuk, A.M., Menon, B.K., Eesa, M., Rempel, J.L., Thornton, J., Roy, D., Jovin, T.G., Willinsky, R.A., Sapkota, B.L., Dowlatshahi, D., Frei, D.F., Kamal, N.R., Montanera, W.J., Poppe, A.Y., Ryckborst, K.J., Silver, F.L., Shuaib, A., Tampieri, D., et al., 2015. Randomized assessment of rapid endovascular treatment of ischemic stroke. N. Engl. J. Med. 372 (11), 1019–1030. https://doi.org/10.1056/nejmoa1414905.
Gu, X., Qi, Y., Erdman, A., Li, Z., 2017. The role of simulation in the design of a semi-enclosed tubular embolus retrieval. J. Med. Devices, Trans. ASME 11 (2), 1–7. https://doi.org/10.1115/1.4036286.
Gültekin, O., Lohr, M.J., Bechtel, G.N., Rausch, M.K., 2024. "What makes blood clots break off?" A back-of-the-envelope computation toward explaining clot embolization. Cardiovasc. Eng. Technol. 15 (5), 584–593. https://doi.org/10.1007/s13239-024-00733-2.
Gunning, G.M., McArdle, K., Mirza, M., Duffy, S., Gilvarry, M., Brouwer, P.A., 2018. Clot friction variation with fibrin content; implications for resistance to thrombectomy. J. Neurointerventional Surg. 10 (1), 34–38. https://doi.org/10.1136/neurintsurg-2016-012721.
Johnson, S., Chueh, J., Gounis, M.J., McCarthy, R., Patrick McGarry, J., McHugh, P.E., Gilvarry, M., 2020. Mechanical behavior of in vitro blood clots and the implications for acute ischemic stroke treatment. J. Neurointerventional Surg. 12 (9), 853–857. https://doi.org/10.1136/neurintsurg-2019-015489.
Johnson, S., McCarthy, R., Gilvarry, M., McHugh, P.E., McGarry, J.P., 2021. Investigating the mechanical behavior of clot analogues through experimental and computational analysis. Ann. Biomed. Eng. 49 (1), 420–431. https://doi.org/10.1007/s10439-020-02570-5.
Jovin, T.G., Chamorro, A., Cobo, E., de Miquel, M.A., Molina, C.A., Rovira, A., San Román, L., Serena, J., Abilleira, S., Ribó, M., Millán, M., Urra, X., Cardona, P., López-Cancio, E., Tomasello, A., Castaño, C., Blasco, J., Aja, L., Dorado, L., et al., 2015. Thrombectomy within 8 hours after symptom onset in ischemic stroke. N. Engl. J. Med. 372 (24), 2296–2306. https://doi.org/10.1056/nejmoa1503780.
Kaesmacher, X.J., Boeckh-Behrens, T., Simon, S., Maegerlein, C., Kleine, J.F., Zimmer, C., Schirmer, L., Poppert, H., Huber, T., 2017. Risk of thrombus fragmentation during endovascular stroke treatment. Am. J. Neuroradiol. 38 (5), 991–998. https://doi.org/10.3174/ajnr.A5105.
Kim, S.K., Yoon, W., Kim, T.S., Kim, H.S., Heo, T.W., Park, M.S., 2015. Histologic analysis of retrieved clots in acute ischemic stroke: correlation with stroke etiology and gradient-echo MRI. Am. J. Neuroradiol. 36 (9), 1756–1762. https://doi.org/10.3174/ajnr.A4402.
Kim, O.V., Litvinov, R.I., Alber, M.S., Weisel, J.W., 2017. Quantitative structural mechanobiology of platelet-driven blood clot contraction. Nat. Commun. 8 (1), 1–10. https://doi.org/10.1038/s41467-017-00885-x.
Kolling, S., Du Bois, P.A., Benson, D.J., Feng, W.W., 2007. A tabulated formulation of hyperelasticity with rate effects and damage. Comput. Mech. 40 (5), 885–899. https://doi.org/10.1007/s00466-006-0150-x.
Krasokha, N., Theisen, W., Reese, S., Mordasini, P., Brekenfeld, C., Gralla, J., Slotboom, J., Schrott, G., Monstadt, H., 2010. Mechanical properties of blood clots - a new test method. Mater. Werkst. 41 (12), 1019–1024. https://doi.org/10.1002/mawe.201000703.
Liang, X., Chernysh, I., Purohit, P.K., Weisel, J.W., 2017. Phase transitions during compression and decompression of clots from platelet-poor plasma, platelet-rich plasma and whole blood. Acta Biomater. 60, 275–290. https://doi.org/10.1016/j.actbio.2017.07.011.
Litvinov, R.I., Weisel, J.W., 2023. Blood clot contraction: mechanisms, pathophysiology, and disease. Res. Pract. Thrombosis Haemostasis 7 (1), 100023. https://doi.org/10.1016/j.rpth.2022.100023.
Liu, R., Jin, C., Wang, L., Yang, Y., Fan, Y., Wang, W., 2022. Simulation of stent retriever thrombectomy in acute ischemic stroke by finite element analysis. Comput. Methods Biomech. Biomed. Eng. 25 (7), 740–749. https://doi.org/10.1080/10255842.2021.1976761.
Liu, S., Bao, G., Ma, Z., Kastrup, C.J., Li, J., 2021. Fracture mechanics of blood clots: measurements of toughness and critical length scales. Extreme Mech. Lett. 48, 12–14. https://doi.org/10.1016/j.eml.2021.101444.
Liu, S., Bhamani, A., Sugerman, G.P., Yang, Z., Rausch, M., Ghezelbash, F., Li, J., 2024. Adhesive and cohesive fracture of blood clots: experiments and modeling. J. Mech. Phys. Solid. 193 (May), 105858. https://doi.org/10.1016/j.jmps.2024.105858.
Liu, Y., Reddy, A.S., Cockrum, J., Ajulufoh, M.C., Zheng, Y., Shih, A.J., Pandey, A.S., Savastano, L.E., 2020. Standardized fabrication method of human-derived emboli with histologic and mechanical quantification for stroke research. J. Stroke Cerebrovasc. Dis. 29 (11), 105205. https://doi.org/10.1016/j.jstrokecerebrovasdis.2020.105205.
Lohr, M., Bechtel, G., Rausch, M., 2024. How to measure fracture toughness of soft materials : a comparison of six different approaches using blood clot as a model material how to measure. Fracture Toughness of Soft Materials : A Comparison of Six.
Luraghi, G., Bridio, S., Lissoni, V., Dubini, G., Dwivedi, A., McCarthy, R., Fereidoonnezhad, B., McGarry, P., Gijsen, F.J.H., Rodriguez Matas, J.F., Migliavacca, F., 2022a. Combined stent-retriever and aspiration intra-arterial thrombectomy performance for fragmentable blood clots: a proof-of-concept computational study. J. Mech. Behav. Biomed. Mater. 135 (June), 105462. https://doi.org/10.1016/j.jmbbm.2022.105462.
Luraghi, G., Bridio, S., Migliavacca, F., Rodriguez Matas, J.F., 2022b. Self-expandable stent for thrombus removal modeling: solid or beam finite elements? Med. Eng. Phys. 106 (January), 103836. https://doi.org/10.1016/j.medengphy.2022.103836.
Luraghi, G., Bridio, S., Miller, C., Hoekstra, A., Rodriguez Matas, J.F., Migliavacca, F., 2021a. Applicability analysis to evaluate credibility of an in silico thrombectomy procedure. J. Biomech. 126 (July), 110631. https://doi.org/10.1016/j.jbiomech.2021.110631.
Luraghi, G., Bridio, S., Rodriguez Matas, J.F., Dubini, G., Boodt, N., Gijsen, F.J.H., van der Lugt, A., Fereidoonnezhad, B., Moerman, K.M., McGarry, P., Konduri, P.R., Arrarte Terreros, N., Marquering, H.A., Majoie, C.B.L.M., Migliavacca, F., 2021b. The first virtual patient-specific thrombectomy procedure. J. Biomech. 126 (July). https://doi.org/10.1016/j.jbiomech.2021.110622.
Luraghi, G., Migliavacca, F., Rodriguez Matas, J.F., 2018. Study on the accuracy of structural and FSI heart valves simulations. Cardiovasc. Eng. Technol. 9 (4), 723–738. https://doi.org/10.1007/s13239-018-00373-3.
Luraghi, G., Rodriguez Matas, J.F., Dubini, G., Berti, F., Bridio, S., Duffy, S., Dwivedi, A., McCarthy, R., Fereidoonnezhad, B., McGarry, P., Majoie, C.B.L.M., Migliavacca, F., 2021c. Applicability assessment of a stent-retriever thrombectomy finite-element model. Interface Focus 11 (1), 20190123. https://doi.org/10.1098/rsfs.2019.0123.
Machi, P., Jourdan, F., Ambard, D., Reynaud, C., Lobotesis, K., Sanchez, M., Bonafé, A., Costalat, V., 2017. Experimental evaluation of stent retrievers' mechanical properties and effectiveness. J. Neurointerventional Surg. 9 (3), 257–263. https://doi.org/10.1136/neurintsurg-2015-012213.
Malone, F., McCarthy, E., Delassus, P., Fahy, P., Kennedy, J., Fagan, A.J., Morris, L., 2018. The mechanical characterisation of bovine embolus analogues under various loading conditions. Cardiovasc. Eng. Technol. 9 (3), 489–502. https://doi.org/10.1007/s13239-018-0352-3.
Mousavi, J.S.S.M., Faghihi, D., Sommer, K., Bhurwani, M.M.S., Patel, T.R., Santo, B., Waqas, M., Ionita, C., Levy, E.I., Siddiqui, A.H., Tutino, V.M., 2021. Realistic computer modelling of stent retriever thrombectomy: a hybrid finite-element analysis-smoothed particle hydrodynamics model. J. R. Soc. Interface 18 (185). https://doi.org/10.1098/rsif.2021.0583.
Saver, J.L., Goyal, M., Bonafe, A., Diener, H.-C., Levy, E.I., Pereira, V.M., Albers, G.W., Cognard, C., Cohen, D.J., Hacke, W., Jansen, O., Jovin, T.G., Mattle, H.P., Nogueira, R.G., Siddiqui, A.H., Yavagal, D.R., Baxter, B.W., Devlin, T.G., Lopes, D.K., et al., 2015. Stent-retriever thrombectomy after intravenous t-PA vs. t-PA alone in

stroke. N. Engl. J. Med. 372 (24), 2285–2295. https://doi.org/10.1056/nejmoa1415061.

Sporns, P.B., Jeibmann, A., Minnerup, J., Broocks, G., Nawabi, J., Schön, G., Fiehler, J., Wildgruber, M., Heindel, W., Kemmling, A., Hanning, U., 2019. Histological clot composition is associated with preinterventional clot migration in acute stroke patients, 2065–2071. https://doi.org/10.1161/STROKEAHA.118.023314.

Staessens, S., De Meyer, S.F., 2021. Thrombus heterogeneity in ischemic stroke. Platelets 32 (3), 331–339. https://doi.org/10.1080/09537104.2020.1748586.

Sugerman, G.P., Parekh, S.H., Rausch, M.K., 2020. Nonlinear, dissipative phenomena in whole blood clot mechanics. Soft Matter 16 (43), 9908–9916. https://doi.org/10.1039/d0sm01317j.

Tutwiler, V., Litvinov, R.I., Lozhkin, A.P., Peshkova, A.D., Lebedeva, T., Ataullakhanov, F.I., Spiller, K.L., Cines, D.B., Weisel, J.W., 2016. Kinetics and mechanics of clot contraction are governed by the molecular and cellular composition of the blood. Blood 127 (1), 149–159. https://doi.org/10.1182/blood-2015-05-647560.

Tutwiler, V., Maksudov, F., Litvinov, R.I., Weisel, J.W., Barsegov, V., 2021. Strength and deformability of fibrin clots: biomechanics, thermodynamics, and mechanisms of rupture. Acta Biomater. 131, 355–369. https://doi.org/10.1016/j.actbio.2021.06.046.

Tutwiler, V., Singh, J., Litvinov, R.I., Bassani, J.L., Purohit, P.K., Weisel, J.W., 2020. Rupture of blood clots: mechanics and pathophysiology. Sci. Adv. 6 (35), 2–10. https://doi.org/10.1126/sciadv.abc0496.

Ye, G., Cao, R., Lu, J., Qi, P., Hu, S., Chen, K., Tan, T., Chen, J., Wang, D., 2021. Histological composition behind CT-based thrombus density and perviousness in acute ischemic stroke. Clin. Neurol. Neurosurg. 207 (March), 106804. https://doi.org/10.1016/j.clineuro.2021.106804.

Yoo, A.J., Andersson, T., 2017. Thrombectomy in acute ischemic stroke: challenges to procedural success. J. Stroke 19 (2), 121–130. https://doi.org/10.5853/jos.2017.00752.

Yuki, I., Kan, I., Vinters, H.V., Kim, R.H., Golshan, A., Vinuela, F.A., Sayre, J.W., Murayama, Y., Vinuela, F., 2012. The impact of thromboemboli histology on the performance of a mechanical thrombectomy device. Am. J. Neuroradiol. 33 (4), 643–648. https://doi.org/10.3174/ajnr.A2842.